Atmospheric Research 342 (2026) 109101

Contents lists available at ScienceDirect

Atmospheric Research

journal homepage: www.elsevier.com/locate/atmosres

Effects of aerosol on microphysical processes and precipitation in an extreme rainfall case of South China: A numerical study

Hong Wang [a,b], Ming Xue [c,*], Jinfang Yin [d,e], Hua Deng [a]

[a] *Guangzhou Institute of Tropical and Marine Meteorology/Guangdong Provincial Key Laboratory of Regional Numerical Weather Prediction, CMA, Guangzhou 510641, China*

[b] *Key Laboratory of Mesoscale Severe Weather, Ministry of Education and School of Atmospheric Sciences, Nanjing University, Nanjing, China*

[c] *Center for Analysis and Prediction of Storms and School of Meteorology, University of Oklahoma, Norman, OK, USA*

[d] *State Key Laboratory of Severe Weather Meteorological Science and Technology, Chinese Academy of Meteorological Sciences, Beijing 100081, China*

[e] *Shigatse National Climatological Observatory, CMA, Shigatse 857000, China*

ARTICLE INFO

Keywords:
Aerosol and CCN
Microphysics scheme
Warm-rain processes
Heavy rainfall

ABSTRACT

This study investigates the impacts of aerosols on the warm-rain and ice-phase microphysics processes within a warm-sector extreme rainfall event that occurred on May 6–7, 2017 over the Guangdong-Hong Kong-Macao Greater Bay Area. The WRF model coupled with the Thompson aerosol-aware bulk microphysics scheme is used. Simulations with varying cloud condensation nuclei (CCN) concentrations successfully reproduce the general spatial pattern of the observed extreme rainfall, with relatively small location and intensity errors. The simulated precipitation decreases with increase in the CCN concentrations. Compared to a low-CCN scenario (in CCNm01, with surface CCN at 25 cm^{-3} that is about 10% of typical maritime values), the high-CCN scenario (in CCNc10, with surface CCN at 10^4 cm^{-3} or about 10 times of typical continental values) shows a 10% reduction in total rainfall and a 1.5–2 mm h^{-1} decrease in early-stage hourly rainfall intensity. High CCN concentrations significantly increase the number of cloud droplets through activation, leading to much smaller droplet sizes and less efficient auto-conversion and accretion/coalescence, resulting in reduced raindrop mass and number. This inefficiency permits more cloud droplets to rise above the freezing level, enhancing ice microphysical processes—including freezing, riming, and deposition. Snow and graupel masses increase, with snow mixing ratios rising by ~25%. However, the aerosol effects on ice-phase processes are less compared to warm-rain processes, and rainfall is more affected by the altered warm-rain processes.

1. Introduction

Over the past few decades, emissions of anthropogenic aerosols increase with rapid industrialization and urbanization. Simulation results from the Goddard Chemistry Aerosol Radiation and Transport (GOCART) model show that, the concentration of anthropogenic aerosols (e. g., sulfates and black carbon) is comparable to that of natural aerosols (e. g., sea salt), especially in East Asia (Thompson and Eidhammer, 2014). Direct observations from several sites indicate that the anthropogenic aerosols can increase cloud condensation nuclei concentrations (CCN) by 100 times (Rosenfeld et al., 2008), which cause a much greater impact on cloud height than the natural aerosols (Jiang et al., 2018). Numerous studies (Rosenfeld et al., 2008; Tao et al., 2012; Fan et al., 2016; Li et al., 2017) indicate that the impact of aerosols on global weather and climate cannot be ignored, yet the mechanisms underlying these effects remain insufficiently clear. Aerosols affect weather and climate through aerosol-radiation interactions (Twomey, 1977) and aerosol-cloud interactions (Glotfelty et al., 2019; Chen et al., 2021). The former represents a direct effect, where aerosols reflect or absorb solar radiation, alter the atmospheric energy balance and thereby cause temperature changes. The latter is an indirect effect, including the "Twomey" effect (Twomey et al., 1984), in which more aerosols lead to more cloud droplets with smaller sizes for a constant liquid water path, and second indirect effect (Fan et al., 2016), which predominantly impacts cloud extent and lifetime.

Precipitation plays an important role in the water and energy cycles. The formation of precipitation and the release of latent heating is closely related to cloud microphysical processes. Aerosols can act as CCN and

* Corresponding author.
E-mail address: mxue@ou.edu (M. Xue).

https://doi.org/10.1016/j.atmosres.2026.109101
Received 22 December 2025; Received in revised form 9 April 2026; Accepted 19 May 2026
Available online 20 May 2026
0169-8095/© 2026 Published by Elsevier B.V.

ice nuclei (IN) to regulate cloud microphysical processes (Ramanathan et al., 2001). Therefore, meteorologists have carried out extensive research on aerosol-precipitation interactions and have proposed a well-known theory stating that a higher concentration of aerosols inhibits the warm cloud process (Albrecht, 1989; Rosenfeld et al., 2008). There are two reasons for this. First, the “Twomey” effect leads to smaller cloud droplet sizes, and the key warm cloud processes (such as auto-conversion and collision-coalescence) for raindrop formation depend on droplet sizes (Berry and Reinhardt, 1974). Second, the condensation growth equation shows that smaller droplets grow more quickly, so a higher concentration of CCN leads to a narrower cloud droplet spectrum (Tao et al., 2012). Meanwhile, more cloud droplets are lifted above the freezing level, promote more active ice-phase processes (such as droplet freezing, riming, and deposition), which release more latent heating of fusion and strengthen convection (Rosenfeld et al., 2008; Zhang et al., 2021). These processes are more pronounced in environments where the cloud base is relatively warm (>15 °C) and vertical wind shear is weak (Fan et al., 2009; Fan et al., 2012; Lebo et al., 2012).

Subsequent studies (Khain et al., 2008; Fan et al., 2016; Liu et al., 2024) have shown that aerosol impacts on cloud properties and precipitation are highly complex and strongly dependent on cloud types and environmental conditions. Thermodynamic and dynamic factors, such as wind shear, relative humidity, and convective available potential energy (CAPE), play important roles in modulating aerosol effects. For example, precipitation responses are closely linked to cold pool intensity and environmental humidity, with aerosols tending to enhance precipitation in moist environments (Tao et al., 2007; Khain et al., 2008). Although CAPE is often the primary control on precipitation intensity, aerosols can still substantially modify microphysical processes and account for a significant fraction of precipitation variability (Storer et al., 2010). The aerosol effect is also sensitive to dynamical structure. Fan et al. (2009) emphasized that vertical wind shear can modulate the aerosol effect in isolated convective clouds, with aerosols tending to inhibit (enhance) convection in strong (weak) vertical wind shear environments. However, for mesoscale convective systems (MCS), aerosols promote convection below 8 km height regardless of shear conditions (Chen et al., 2020). Additionally, the aerosol effect varies with height within convective system, with the warming effect near the cloud base being 2–3 times stronger than in mixed-phase regions (Lebo, 2018). In the East Asian monsoon region, aerosols also significantly influence cloud microphysics and precipitation intensity, affecting droplet formation, ice processes, and autoconversion (Fan et al., 2012; Jiang et al., 2016; Cao et al., 2021).

Warm-sector heavy rainfall (WR) is a common extreme weather phenomenon in southern China. Unlike typical frontal rainfall, WR often occurs with weaker synoptic or meso-scale forcing. Its cloud microphysical processes and heavy rainfall mechanisms are more complex (Luo et al., 2017; Wu et al., 2020; Han et al., 2021; Feng et al., 2023). The aerosol impact on cloud and precipitation mechanisms in WR is less clear. Meanwhile, the Guangdong-Hong Kong-Macau Greater Bay Area, as one of the world's largest urban agglomerations, has significant anthropogenic aerosol emissions (Zhang et al., 2010). Therefore, it is essential to carry out research on the impact of aerosols on urban extreme precipitation in the region.

On May 6–7, 2017, a local extreme heavy rainfall event occurred in Guangzhou, with a maximum cumulative rainfall of 543 mm over 17 h (Wang et al., 2023b). This study will employ the Weather Research and Forecasting (WRF) cloud-resolving model coupled with the Thompson Aerosol-Aware microphysics scheme (THOM-Aero, (Thompson and Eidhammer, 2014)) to investigate the impacts of anthropogenic aerosols on this extreme rain event. A series of numerical experiments are designed to quantify how variations in aerosol concentration influence precipitation, convective intensity, and cloud microphysical characteristics. The analysis focuses on the aerosol-induced changes in both warm-rain and ice-phase processes, with particular attention to the pathways through which aerosols modulate the formation of cloud and precipitation. Specifically, we address the following questions: (1) How do aerosols influence the formation, growth, and phase transition of hydrometeors? (2) How do these microphysical perturbations translate into changes in convective intensity and rainfall characteristics?

The rest of this paper is organized as follows. Section 2 details the data and model configuration. Section 3 presents the results about the impacts of aerosols on warm-rain and ice phase processes. The discussion and conclusion are given in the Section 4.

2. Data and model configuration

2.1. Case description

During 6–7 May 2017, an extreme rainfall event occurred in the Guangdong-Hong Kong-Macao Greater Bay Area (GBA, Fig. 1 black curve), which is the largest and most populated urban area in the world. Its precipitation showed obvious mesoscale characteristics including large hourly intensity and long duration (Xu et al., 2018). The maximum hourly rainfall rate of 184 mm h^{-1} occurred at Jiulong (Fig. 1 blue dot), where rainfall exceeding 20 mm h^{-1} persisted for 9 h. Fig. 1 presents a weather chart at 1200 UTC 6 May 2017, which was 3–4 h prior to the convective initiation of this case. The GBA was dominated by southerly winds with speeds of 2–4 m s^{-1} at 900 hPa, accompanied by abundant moisture. Notably, precipitable water in the main precipitation area (Fig. 1 red box) exceeded 56 mm. In the mid-troposphere, the GBA was located at the edge of the subtropical high (not shown). The CAPE observed at the Hong Kong sounding station was about 1503 J kg^{-1}. In brief, this extreme rain occurred in a high humidity environment without obvious synoptic weather forcing (Xu et al., 2018), and is therefore a WR case.

2.2. Model description

We conduct model simulations using the WRF Model version 3.9.1. All model configurations, except for the microphysics scheme, are consistent with those of Yin et al. (2020). The details can be found in Section 3 from their paper. The grid configurations are as follows: the simulations are configured with two-way interactive, triply nested domains with the horizontal grid spacings of 12, 4, and 1.33 km. The innermost two domains (i.e., D02 and D03) are also shown in the Fig. 1. The grid has 57 vertical levels with vertical stretching below 850 hPa

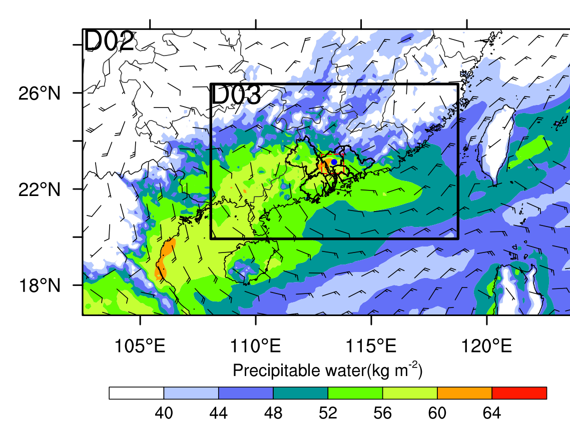

Fig. 1. The precipitable water (kg m^{-2}, shadings) and wind barbs (a full barb is 4 m s^{-1}) at 900 hPa from the National Centers for Environmental Prediction Global Forecast System Final (NCEP-FNL) analysis at 1200 UTC 6 May 2017. The black rectangles denote the nested model domains used for the WRF simulations with the grid resolution of 4 km (D02) and 1.33 km (D03), respectively. The red box and blue dot indicate the main precipitation area and Jiulong station. The black curve shows the administrative area of the Guangdong-Hong Kong-Macao Greater Bay Area. (For interpretation of the references to colour in this figure legend, the reader is referred to the web version of this article.)

and above 200 hPa. All three nested domains are integrated for 18 h, starting from 1200 UTC 6 May, with outputs at 6-min intervals. All simulations use the following physics parameterizations: the rapid radiative transfer model (Mlawer et al., 1997) for both shortwave and longwave, the Yonsei University PBL scheme (Hong et al., 2006), the MM5 Monin–Obukhov similarity surface-layer scheme (Zhang and Anthes, 1982), the Noah-MP land surface scheme (Niu et al., 2011), and the cumulus parameterization scheme (Kain, 2004) in the two outer coarse-resolution domains only. The microphysics scheme used will be discussed in the next subsection.

The initial and boundary conditions are derived from the NCEP GFS Final Analysis (FNL) 0.25° data with a temporal resolution of 6 h. Considering the importance of the urban heat island on convective initiation of this case (Xu et al., 2018; Wang et al., 2023b), we apply observation nudging (Seaman et al., 1995) towards hourly surface observations between 1200 UTC 6 May and 0000 UTC 7 May 2017, to realistically simulate the urban heat island effects. The same procedure was used in Wang et al. (2023a) for the simulation of this case.

2.3. Experiment configurations

Most pertinent to this study, we use the THOM-Aero scheme to investigate aerosol effect on heavy rainfall over South China. In our previous study (Wang et al., 2023a), regular Thompson bulk microphysics scheme (Thompson et al., 2008) demonstrated a good performance in simulating this WR event. When compared with polarimetric radar observations, the Thompson scheme reasonably reproduced the median raindrop size and number concentration, outperforming the other two schemes (i.e., NSSL and Morrison). The Thompson scheme treats five separate water species: cloud water, cloud ice, rain, snow, and a hybrid graupel–hail category. This scheme utilizes one-moment prediction of mass mixing ratio for snow and graupel mixed with two-moment predictions (with the addition of number concentrations) of cloud water, cloud ice and rain. To address the complex and uncertain problem of aerosol effects, the original Thompson scheme was updated to incorporate the activation of aerosols as CCN and IN in the THOM-Aero version. Compared to the original Thompson scheme, THOM-Aero with its three additional variables (i.e., cloud droplet number concentration, number of each aerosol species "water friendly" and "ice friendly") increases computational cost by approximately 16%. Therefore, the THOM-Aero scheme, with its great potential for operational applications and good performance in previous studies (Thompson and Eidhammer, 2014; Rasmussen et al., 2020), is used in this study to study the aerosol effects on clouds and precipitation.

In the THOM-Aero scheme, initial "water friendly" aerosol conditions are given by exponentially decreasing profile of concentration from the surface to 2 km and constant amount above (Thompson and Eidhammer, 2014). For example, a typical maritime profile has a surface aerosol concentration of 250 cm^{-3} that decreases to 50 cm^{-3} aloft (blue line in Fig. 2, used in experiment CCNm) and a typical continental profile starts with 1000 cm^{-3} near the surface and decreases to 250 cm^{-3} aloft (dark green line in Fig. 2, used in experiment CCNc). To test the sensitivity to the initial aerosol concentrations, two more experiments are conducted. Experiment CCNm01 (purple line in Fig. 2) represents extremely clean scenario with concentrations reduced to one-tenth of CCNm, while experiment CCNc10 (red brown line in Fig. 2) represents heavy anthropogenic aerosol scenario with aerosol concentrations increased tenfold compared to CCNc. The choice of these CCN perturbation magnitudes (one tenth and ten times) follow the experimental design of Jiang et al. (2016), who investigated aerosol impacts on typhoon precipitation and microphysical processes using WRF-Chem and adopted similar scaling factors to represent clean and heavily polluted environments. In May 2017, the PM2.5 and PM10 concentrations in Guangzhou were approximately 40 and 60 μg m^{-3}, respectively (available at https://sthjj.gz.gov.cn/zwgk/hjgb/content/post_2808233.html), indicating a moderately polluted urban environment.

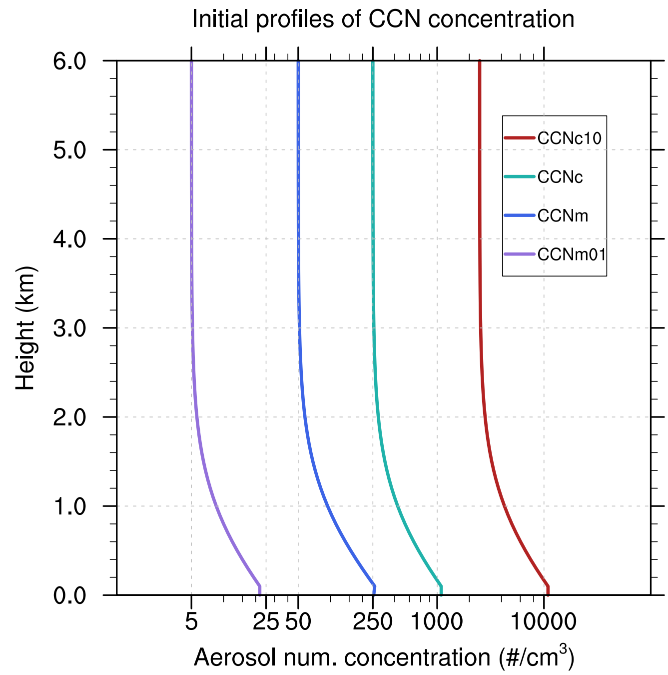

Fig. 2. Initial profiles of the total number concentration of aerosol particles (unit: cm^{-3}) for experiments CCNc10, CCNc, CCNm and CCNm01.

Observational studies suggest that under typical supersaturation conditions, such pollution levels generally correspond to CCN on the order of $\sim 10^3$ cm^{-3}. Therefore, the CCNc experiment is likely closest to the actual aerosol conditions in this case. The default "ice friendly" aerosol profiles from Thompson and Eidhammer (2014) are retained in this study to isolate CCN effects, although regional aerosol characteristics over South China may differ and introduce some uncertainty. For "water-friendly" aerosols, the sink terms include CCN activation, collection by rain, snow, graupel, as well as homogeneous nucleation deliquescence, whereas source terms arise from cloud and rain evaporation and surface emissions. In contrast, for "ice-friendly" aerosols, the sink terms consist IN activation and collection by rain, snow, graupel, while the source terms include cloud ice sublimation and surface emission. The detailed descriptions of these source and sink processes are provided in Section 2 of Thompson and Eidhammer (2014).

3. Results

3.1. Model evaluation

Fig. 3 show the observed and simulated 17-h accumulated rainfall. In general, all experiments reproduce reasonably well the general pattern of heavy rainfall. The rainfall exceeding 150 mm are all located in the central part of Guangzhou, with the predicted maximum precipitation position deviating from the observed location by approximately 20 km to the east. Because of the use of global model analyses as the initial and boundary conditions for the simulations, and the lack of data assimilation including local data, such relatively small position errors are difficult to avoid. For the purposes of our current study that focuses on physical processes rather than forecast accuracy, the ~20 km position error is deemed acceptable. It is also on par with errors in previous simulation studies on this case (Wang et al., 2023a).

There are further differences in predicted precipitation magnitudes. The maximum accumulated rainfall decreases as the aerosol concentration increases. Experiment CCNm01 (Fig. 3d) simulates a maximum accumulation of 552 mm, close to the observed 543 mm but experiment CCNc10 (Fig. 3a) produces the lowest maximum accumulation of 443 mm. To explore the evolution of precipitation and quantify the impact of

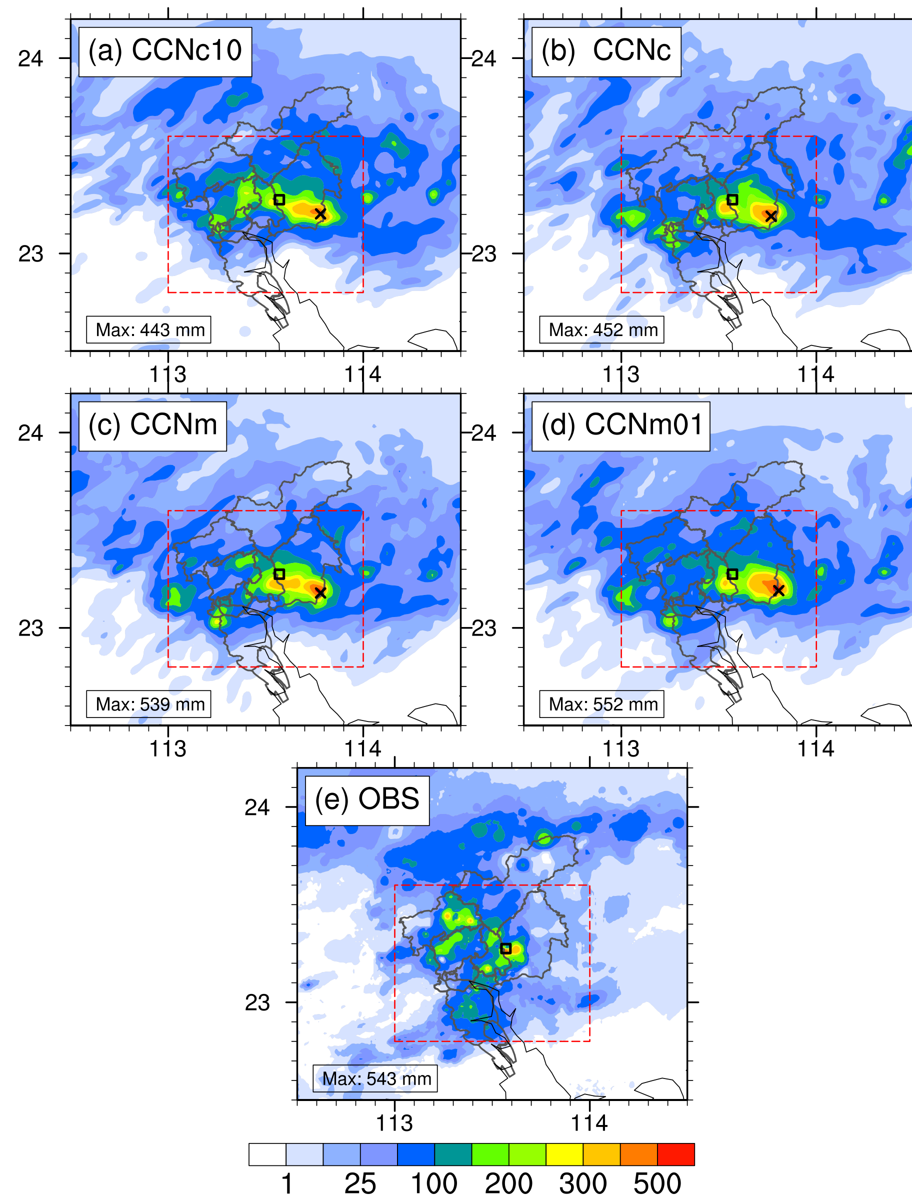

Fig. 3. The simulated (a)–(d) and observed (e) total precipitation (unit: mm) from 1600 UTC 6 May to 0700 UTC 7 May. The black small square box and the cross represent the locations of maximum observed and simulated total precipitation, respectively. The maximum total precipitation is provided in the bottom-left-hand corner of the panel. The red dashed box in each panel is used for diagnostic calculations. The horizontal and vertical axis labels are in longitude and latitude degrees. (For interpretation of the references to colour in this figure legend, the reader is referred to the web version of this article.)

aerosol effects on microphysical processes, a specific area indicated by the red dashed box in Fig. 3 (113–114°E, 22.8–23.6°N) is selected for diagnostic calculations.

Hourly precipitation also exhibits a decreasing trend with increasing aerosol concentrations (Fig. 4). All simulations overestimate the regionally averaged hourly precipitation, particularly in the early stages, with values exceeding observations by approximately 1.5–2 mm h^{-1} (Fig. 4a). Systematic model errors such as those related to grid resolution and/or initial condition error might have caused such precipitation intensity errors. In this paper, we focus more on the relative intensity among the experiments that differ only in the initial specified aerosol concentrations. We assume that systematic model errors do not affect the relative intensities related to aerosol concentration differences.

Compared to CCNm01, experiment CCNc10 shows a ~10% reduction in the regionally averaged hourly rain rates.Notably, from 1500 UTC to 2000 UTC on 6 May,CCNc10 produces lower rainfall rates than the other three experiments, suggesting a weakening of precipitation during this period. This trend is also evident in the regionally accumulated total precipitation, where experiment CCNc10 consistently produces lower values than the other three experiments. By 0700 UTC 7 May, the difference between the total precipitations of CCNc10 and CCNm01 reaches 0.6×10^8 tons (Fig. 4c), accounting for about 10% of the total accumulated precipitation. These results indicate that enhanced anthropogenic aerosols suppress precipitation formation. Additionally, both CCNm01 and CCNm show higher occurrences of large precipitation rates (>100 mm h^{-1}) compared to CCNc and CCNc10 (Fig. 4b). The precipitation behavior differs from two previous studies in the same region (Liu et al., 2020; Cao et al., 2021), which investigated the winter precipitation events and found that aerosol effects tended to enhance precipitation.

Fig. 5 shows the vertical distributions of reflectivity over convective and stratus regions from the four simulations and the GZPR radar observations. Following Wang et al. (2019), the convective regions are

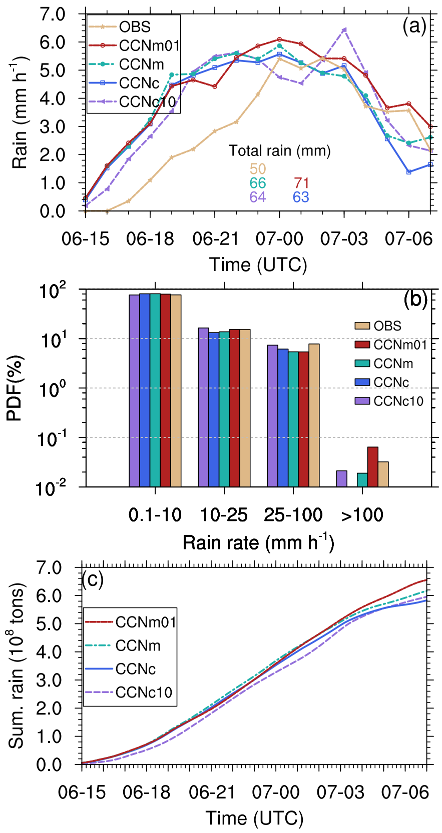

Fig. 4. (a) Time series of the averaged surface rain rate (unit: mm h^{-1}), (b) probability density functions (PDFs) of the rain rate for values larger than 0.1 mm h^{-1} over the study area (red box in Fig. 3) from 1500 UTC on 6 May 2017 to 0700 UTC on 7 May 2017 and (c) Time series of cumulative total precipitation (unit: tons) over the study area. The txt in the bottom of (a) shows mean observed and simulated accumulated precipitations. (For interpretation of the references to colour in this figure legend, the reader is referred to the web version of this article.)

identified according to the vertical extent of reflectivity, while the stratus regions are defined as non-convective grid points with reflectivity greater than 5 dBZ. Overall, the simulated convective reflectivities (Fig. 5a) are weaker than the observations. The mean reflectivity across different experiments varies only slightly, with differences being within 2 dBZ at the same altitude, and even smaller below the 0 °C level. Meanwhile, the standard deviation of reflectivity within the convective region (shaded areas in Fig. 5a) is also smaller below the 0 °C level, indicating higher model accuracy in simulating warm-rain processes. In contrast, the simulation bias and standard deviation in the stratus region (Fig. 5b) are slightly larger than those in the convective region. In particular, the CCNc10 experiment shows a positive bias of nearly 4 dBZ below 3 km height.

The composite profiles of vertical velocity, derived from grid columns where the maximum vertical velocity exceeds 2 m s^{-1} during 2000 UTC 6–0000 UTC 7 May 2017, illustrate the representative vertical structure of convection (Fig. 6). Overall, the average updraft velocity across all experiments ranges from 0.0 to 2.2 m s^{-1}. The vertical profiles exhibit a single-peaked distribution, with the peak occurring approximately 600 m below the 0 °C level. As CCN increases, the updraft shows a slight enhancement. The mean updraft in CCNc10 (purple line in Fig. 6) is about 0.2 m s^{-1} stronger than that in the other experiments in the 2–8 km altitude range. This enhancement can be attributed the increased buoyancy associated with the release of latent heating through microphysical processes. Previous studies (Wu et al., 2018; Zhang et al., 2021) have demonstrated that more aerosols promote the formation of more cloud droplets, leading to additional latent heating release and stronger convective activity. Consequently, stronger updrafts transport more cloud droplets to higher altitudes, facilitating more active ice-phase microphysical processes, such as deposition, drop freezing, and riming. These ice-phase processes release additional latent heat of fusion and further enhance convection above the 0 °C level. It is noteworthy that, the aerosol impact on updrafts in this WR case appears less pronounced than in some of the other cases, such as the frontal MCS case in South China (Cao et al., 2021) and deep convective clouds over Houston, USA (Zhang et al., 2021). The former was associated with strong frontal forcing and organized mesoscale convection, while the latter was triggered by a trailing front and enhanced by surface heating and sea-breeze

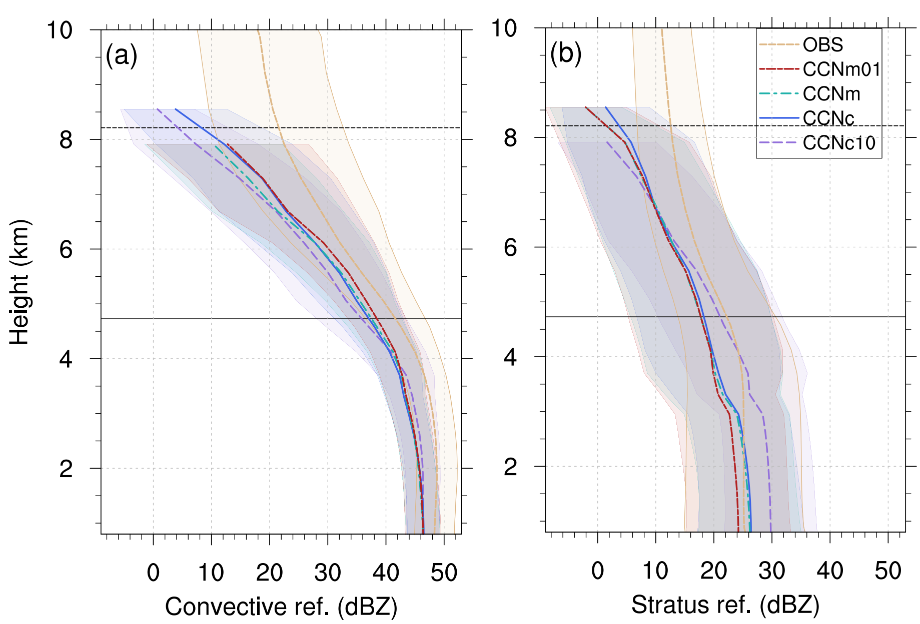

Fig. 5. Composite vertical profiles of average reflectivity (unit: dBZ) over (a) convective and (b) stratus region. The dataset includes the grid columns within the red box shown in Fig. 3, during the period from 2000 UTC 6 to 0000 UTC 7 May 2017. The shaded areas denote ±1 standard deviation from the mean. The profiles are not shown when the sample size is less than 100 in each layer. The black lines indicate the level of 0 °C and −20 °C, respectively. (For interpretation of the references to colour in this figure legend, the reader is referred to the web version of this article.)

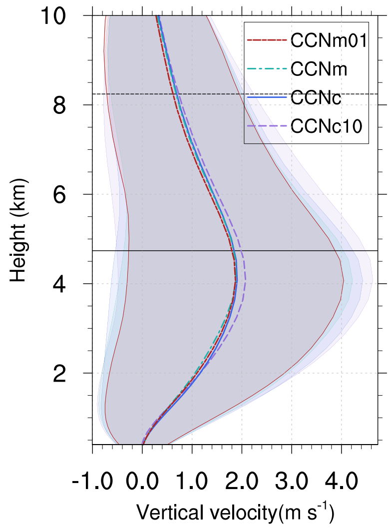

Fig. 6. Composite averaged profiles of vertical velocity (unit: m s^{-1}). The averaging is over grid columns where maximum updraft exceeds 2 m s^{-1} within the red box in Fig. 3, during the period from 2000 UTC 6 to 0000 UTC 7 May 2017. The shaded areas denote ±1 standard deviation from the mean. The profiles are not shown when the sample size is less than 100 in each layer. The black solid and dashed horizontal lines indicate the 0 °C and −20 °C levels, respectively. (For interpretation of the references to colour in this figure legend, the reader is referred to the web version of this article.)

transport of warm, moist air. These environments featured stronger dynamical lifting and localized convective intensification, under which aerosol invigoration effects tend to be more evident.

3.2. Simulated aerosol effects on production of warm rain

We now look at the effects of aerosol concentrations on warm-rain processes further. The hydrometeors involved in the warm-rain processes include cloud water and rainwater. Firstly, the time-height cross sections of mixing ratio and number concentration of cloud water are presented in Fig. 7. Aerosols have little impact on the vertical range and peak altitude of cloud water, which is all located below 10 km height, with the peak mixing ratio occurring at 4 km. The peak number concentration appears at ~2 km, lower than that of mixing ratio. As aerosol concentration increases, the number of cloud droplets rises rapidly, with the maximum values increasing from $10^{6.8}$ kg^{-1} in CCNm01 (Fig. 7d) to $10^{8.4}$ kg^{-1} in CCNc10 (Fig. 7a). Meanwhile, the cloud water mass also increases, but the magnitude of increase is relatively small, by ~35% from CCNm01 to CCNc10. This is related to the cloud processes in the THOM-Aero scheme, where the cloud water mass is closely related to environmental supersaturation, and to auto-conversion and accretion processes that deplete the cloud water. The cloud droplet number concentration is directly related to CCN.

In contrast to the cloud water, both the mass and number concentration of raindrops decrease with the increase in aerosol (Fig. 8). CCNc10 produces maximum rainwater mass of 0.32 g kg^{-1} and number concentration of $10^{3.6}$ kg^{-1} (Fig. 8a), while those in CCNm01 reach 0.42 g kg^{-1} and $10^{4.3}$ kg^{-1} (Fig. 8d). The results of experiments CCNc (Fig. 8b) and CCNm (Fig. 8c) are located inbetween those of CCNc10 and CCNm01. Combining the above results, aerosols promote the formation of more cloud droplets but reduce the formation of raindrops. As in Tao et al. (2012), a higher CCN concentration produces more numerous and uniform cloud droplets, reducing the efficiency of collision–coalescence and thus inhibiting warm-rain formation. Thus, the aerosol effect on the warm-rain processes is manifested as a suppression of precipitation, consistent with previous studies (Albrecht, 1989; Rosenfeld et al., 2008;

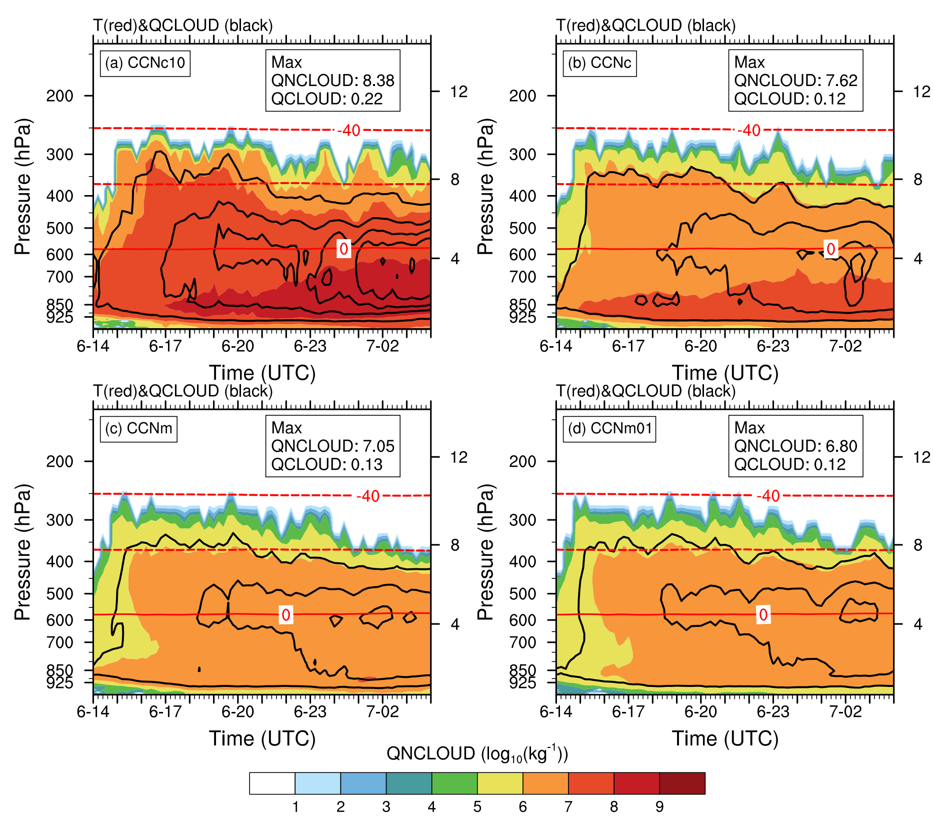

Fig. 7. Time-height cross sections of domain-averaged (over the red box in Fig. 3) number concentration (shaded, unit: $\log_{10}(kg^{-1})$), mixing ratio (black contours start at 0.01 g kg^{-1} with intervals of 0.05 g kg^{-1}) of cloud water, and temperature (red contour lines at 0, −20, −40 °C) from 1400 UTC 6 to 0400 UTC 7 May 2017. (For interpretation of the references to colour in this figure legend, the reader is referred to the web version of this article.)

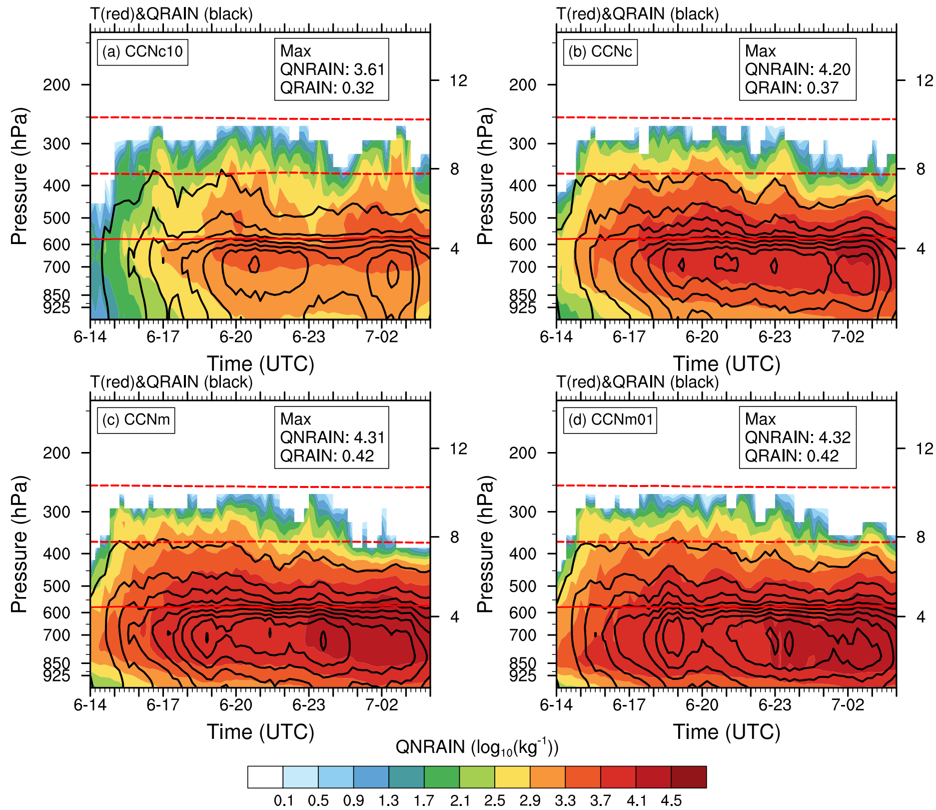

Fig. 8. Same as Fig. 7, but for rain.

Fan et al., 2012).

To further quantify how aerosols suppress warm-rain production, we examine the key microphysical source and sink terms. The calculated tendencies (not shown) indicate that aerosols are mainly consumed through droplet activation, collection by snow, and freezing into cloud ice. Below 8 km altitude, the droplet activation accounts for almost 100%. The domain-averaged (within the red boxes in Fig. 3) and time-averaged (2000 UTC 6 to 0000 UTC 7 May) vertical profiles of droplet activation rate are shown at Fig. 9a. All simulations exhibit similar profile shapes, peaking near 1 km altitude, while the activation rate increases markedly with aerosol loading. In CCNc10, it is nearly two orders of magnitude higher than that in CCNm01, consistent with the distribution of cloud number concentration (Fig. 7). However, the vertical profiles of cloud water condensational growth rate (by mass) show a different behavior (Fig. 10a). The peak appears near the 0 °C level, distinct from the activation maximum. Moreover, the condensation rate does not increase monotonically with aerosol concentration. It increases from CCNm01 to CCNm, but decreases in CCNc and further in CCNc10. The largest difference between CCNm01 and CCNc10 is about 0.06 kg kg^{-1} s^{-1} (about 30%) at ~4 km altitude.

This behavior reflects both scheme constraints and microphysical coupling. In the THOM-Aero scheme (Thompson and Eidhammer, 2014), cloud water mass depends solely on super- or sub-saturation of the air, whereas activation is directly related to CCN. Thus, higher aerosol concentration directly increases droplets number, but their total liquid mass does not increase proportionally. Additionally, ice-phase processes further suppress condensation. In CCNc10, snow and graupel collect more cloud droplets (Fig. 12a and d), enhancing riming and converting liquid water into ice. This reduces the available cloud droplets for condensational growth, contributing to the lower condensation rate. Overall, these results highlight the strong coupling between warm-cloud and ice-phase processes. This is also one of the reasons why cloud droplets tend to be smaller in environments with higher aerosol concentrations.

Subsequently, the cloud droplets from activation are consumed in the processes of auto-conversion (Figs. 9b and 10b) and collection by rain (Figs. 9c and 10c). These two processes also are crucial for the formation and growth of raindrops (Berry and Reinhardt, 1974). Regarding the auto-conversion process, the four experiments exhibit similar results in terms of number concentration (Fig. 9b) and mixing ratio (Fig. 10b). CCNm01 has the most active auto-conversion process, with the peak values of number concentration and mass mixing ratio reaching 2.1×10^5 kg^{-1} s^{-1} and 2.0×10^{-3} kg kg^{-1} s^{-1}, respectively. As aerosol concentration increases, the activity of the auto-conversion process gradually decreases, and the height of the peak also increases. The auto-conversion process in CCNc10 is least active, with peak values of of number concentration and mass mixing ratio reaching 0.2×10^5 kg^{-1} s^{-1} and 0.02×10^{-3} kg kg^{-1} s^{-1}. These values are only one-tenth of those in CCNm01. This can be explained by the smaller particle sizes of cloud droplets in CCNc10, which leads to a reduced efficiency in the auto-conversion process. Consequently, CCNc10 produces the lowest number of raindrops (Fig. 8). These results explain how aerosols inhibit the auto-conversion process in the THOM-Aero scheme. Other microphysics schemes also account for the effect of cloud droplet size on the efficiency of auto-conversion, such as the WRF double-moment 6-class (WDM6) scheme (Lim and Hong, 2012). However, the Morrison scheme (Morrison et al., 2009) does not explicitly account for the dependence of collision efficiency on cloud droplet size. Consequently, in simulation of a MCS over South China using the Morrison scheme, Cao et al. (2021) reported that higher cloud water contents enhanced warm-rain production. In their study, the aerosol effect was manifested as promoting warm-rain processes.

In the four experiments, higher aerosol concentrations result in a greater number of cloud droplets being consumed during the collection process. For example, the peak value in CCNc10 reaches 1.6×10^9 kg^{-1} s^{-1}, which is significantly higher than those in the other three experiments (Fig. 9c). Unlike its significant impact on the number concentration, aerosols have a relatively small effect on the raindrop mass

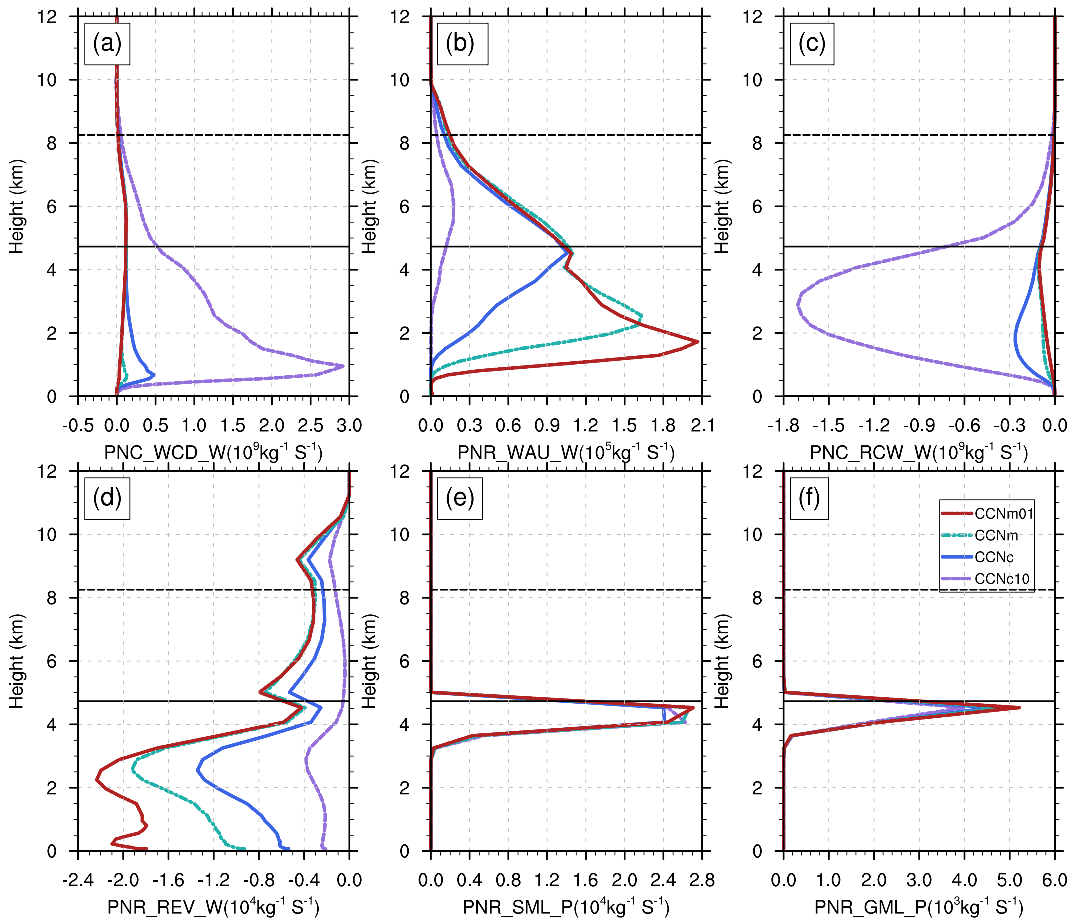

Fig. 9. Regional and temporal mean vertical profiles of number tendency terms associated with major microphysical processes: (a) droplet activation, (b) auto-conversion, (c) rain collecting cloud water, (d) rain evaporation, (e) snow melting, and (f) graupel melting. All values are averaged over the red boxes in Fig. 3 during 2000 UTC 6 to 0000 UTC 7 May. In the horizontal axis notation, "PNX" denotes the number concentration tendency of hydrometeor category X, where "N" represents number concentration and X indicates the corresponding hydrometeor species (i.e., C for cloud droplets and R for rain). Positive and negative values indicate source and sink, respectively. (For interpretation of the references to colour in this figure legend, the reader is referred to the web version of this article.)

during the collection process. In all experiments, the increase in raindrop mass caused by the collection of cloud droplets is similar, with a peak value of 2.7×10^{-3} kg kg^{-1} s^{-1} occurring at a height of ~4 km (Fig. 10c). This is because more aerosols lead to smaller cloud droplet sizes. As a result, even though raindrops collect a large number of cloud droplets, their contribution to total raindrop mass remains limited (i.e., experiment CCNc10).

Meanwhile, evaporation is one of the significant sink terms for raindrops. As is well known, the intensity of evaporation is primarily influenced by the raindrop diameter, with smaller-sized raindrops meaning stronger evaporation (Srivastava and Coen, 1992; Dawson et al., 2010). Due to the more active auto-conversion process, CCNm01 generates more raindrops (Fig. 9b). Meanwhile, its collection process is less active, which inhibits raindrop growth (Fig. 10c). The two processes result in smaller average raindrop diameters in CCNm01, thereby enhancing the evaporation process (Figs. 9d and 10d).

In addition to warm-rain processes, melting of snow and graupel can aslo be important sources of rain production. Snow melting (Figs. 9e and 10e) contributes more significantly than graupel melting (Figs. 9f and 10f). At around 4 km altitude, snow melting contributes approximately 10^{-3} kg kg^{-1} s^{-1} to rainwater mixing ratio and about 2×10^{4} kg^{-1} s^{-1} to rain number concentration. These results suggest that precipitation differences among simulations arise from the combined effects of warm-rain and ice-phase processes. Moreover, the snow melting intensity increases with aerosol loading, likely due to enhanced snow particle production under higher CCN conditions. A more detailed microphysical analysis is provided in the next section.

3.3. Aerosol effects on ice processes

The previous subsection reveals that a higher aerosol concentration results in the formation of more small-sized cloud droplets. Some of these droplets will be transported above the freezing level, where they engage in various ice-phase microphysical processes, such as freezing into cloud ice and collection by snow and graupel. Therefore, in addition to warm-rain processes, aerosols also effect the ice-phase processes to a certain extent. For cloud ice, the freezing of cloud droplets is the primary source of number concentration (i.e., the rate is ~10^{6} kg^{-1} s^{-1}, not shown) but contributes little to its mass. In this case, the mixing ratio of cloud ice is two orders of magnitude smaller than that of snow and graupel. Therefore, we will not focus on the details of cloud ice.

The domain average mixing ratios of snow and graupel are presented in Fig. 11. The snow is distributed between 3.5 and 12 km altitude, with its peak occurring at ~6.5 km. As aerosol concentration increases, the snow also increases, with the peak value rising from 6 g kg^{-1} in CCNm01 to 8 g kg^{-1} in CCNc10 (Fig. 11a). The growth of graupel depends on vertical motion, and the updrafts in CCNc10 are only slightly stronger than those in other experiments (Fig. 6). Consequently, its graupel exhibits a slight increase with peak value of 0.2 g kg^{-1} (Fig. 11b), much smaller than that of snow. Additionally, CCNc10 exhibits higher amounts of snow and graupel below the melting layer than the other experiments. This suggests that the snow and graupel particles in

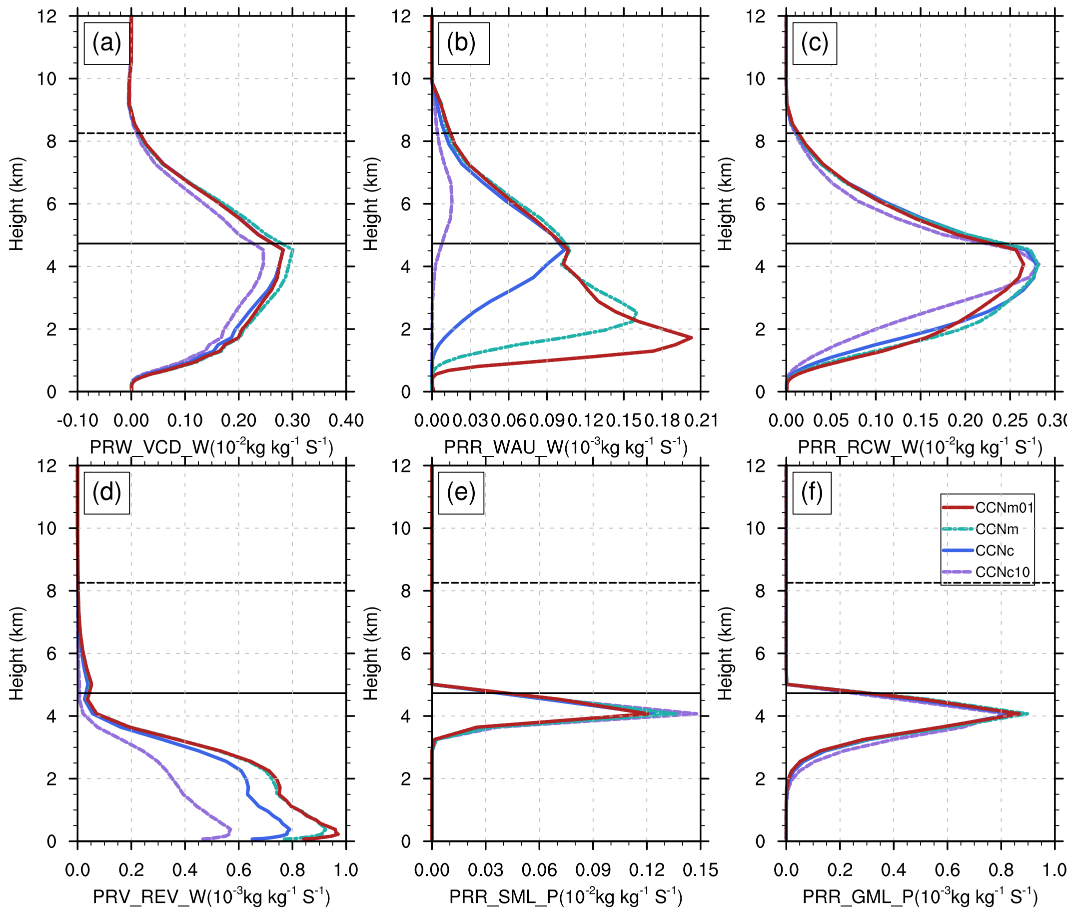

Fig. 10. Regional and temporal mean vertical profiles of mixing ratio tendency terms associated with major microphysical processes (a) cloud water condensation, (b) auto-conversion, (c) rain collecting cloud water, (d) rain evaporation, (e) snow melting, and (f) graupel melting. All the values are averaged over the red boxes in Fig. 3 during 2000 UTC 6 to 0000 UTC 7 May. In the horizontal axis notation, "PRX" denotes the mixing ratio tendency of hydrometeor category X, where "R" represents mixing ratio and X indicates the corresponding hydrometeor species (i.e., W for cloud droplets, R for rain and V for vapor). (For interpretation of the references to colour in this figure legend, the reader is referred to the web version of this article.)

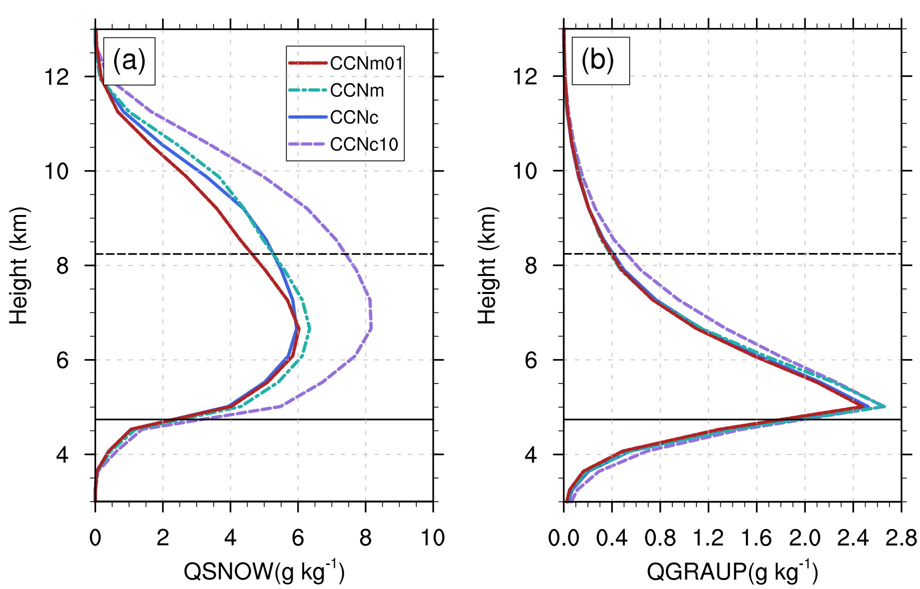

Fig. 11. Vertical profiles of (a) snow and (b) graupel mixing ratio over the delineated red boxes in Fig. 3 during 2000 UTC 6 to 0000 UTC 7 May. (For interpretation of the references to colour in this figure legend, the reader is referred to the web version of this article.)

CCNc10 are larger in size and melt more slowly.

Calculated source and sink terms (not shown) indicate that the three main sources of snow are collection of cloud by snow, deposition of snow and conversion of cloud ice to snow. Their vertical profiles (Fig. 12)

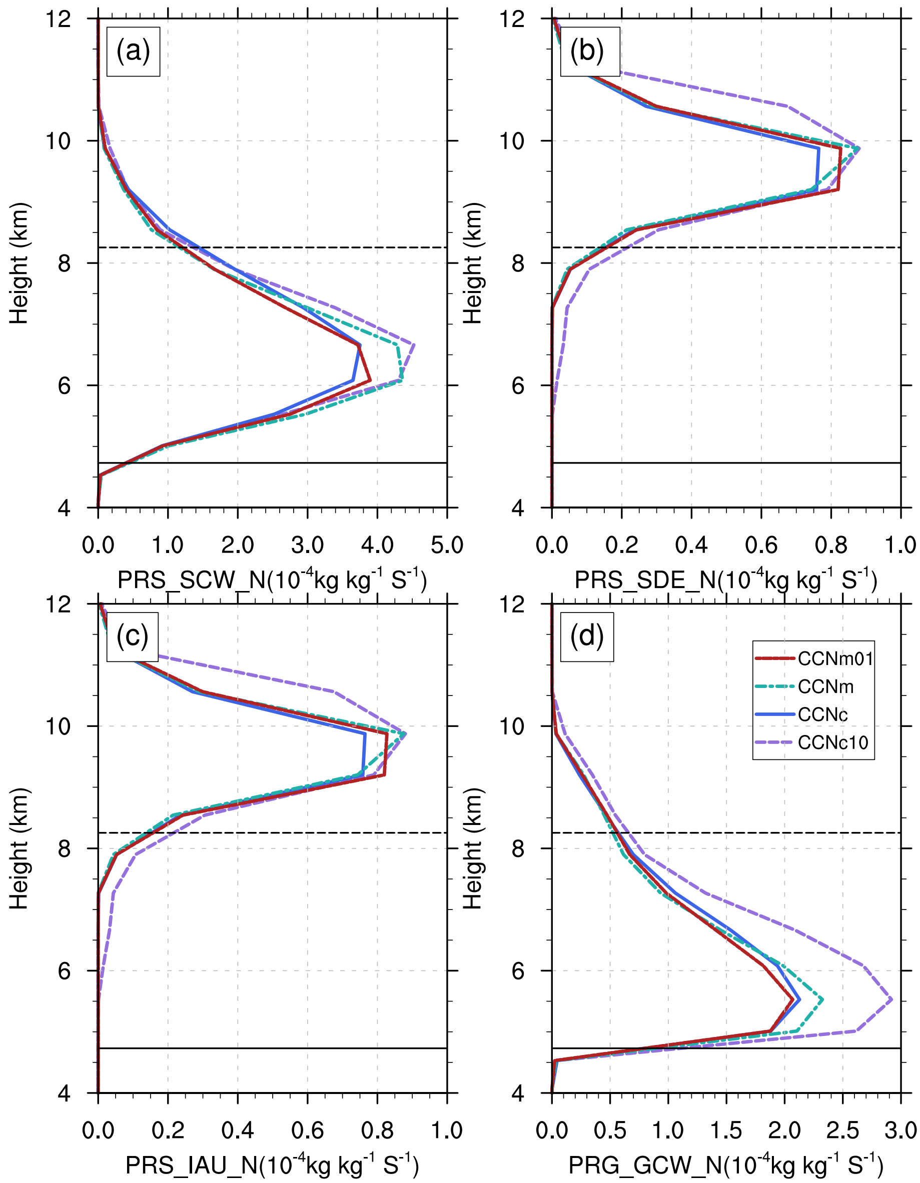

Fig. 12. Vertical profiles of (a) collection of cloud by snow, (b) snow deposition, (c) cloud ice transforming into snow and (d) collection of cloud by graupel over the delineated red boxes in Fig. 3 during 2000 UTC 6 to 0000 UTC 7 May. (For interpretation of the references to colour in this figure legend, the reader is referred to the web version of this article.)

show that collection of cloud by snow is the largest contributor to snow formation. Furthermore, its peak height (i.e., ~6.5 km altitude in Fig. 12a) coincides with the peak height of the snow mixing ratio (Fig. 11a). As aerosol concentration increases, the collection of cloud becomes more active, with the peak value increasing from 0.38×10^{-3} to 0.42×10^{-3} kg kg^{-1} s^{-1} (~10%). The profiles of deposition (Fig. 12b) and conversion (Fig. 12c) are very similar, with their peak heights appearing at ~9 km altitude. However, their magnitudes are an order of magnitude smaller than that of collection, and their differences among the four experiments are relatively small. Meanwhile, the graupel in CCNc10 significantly grows through the collection of cloud droplets between 5 and 8 km altitude, with a rate approximately 28% higher than that in CCNm01 (Fig. 12d). Overall, cloud droplets are lifted to altitudes above the freezing level, contribute to snow and graupel growth to some extent. Still, the impact of aerosols on ice-phase processes is less pronounced than that on warm-rain processes.

The above findings indicate that aerosols can enhance ice-phase processes in WR events over South China, particularly those associated with snow. Similar mechanisms have been documented in various regions, where aerosols act as ice-nucleating particles (Li et al., 2013) or alter cloud microphysics via enhanced heterogeneous freezing and depositional growth (Rosenfeld et al., 2008; Lin et al., 2025). Nevertheless, the magnitude and pathways of this enhancement may vary depending on meteorological conditions (Zhao et al., 2018), aerosol composition (Han et al., 2022), and cloud type (Fan et al., 2016).

4. Conclusions and discussion

This study focuses on a warm-sector heavy rainfall event that occurring on 6–7 May 2017 over the Guangdong–Hong Kong–Macao Greater Bay Area, which produced extreme total precipitation of 543 mm within 16 h. Because this is a major industrialized megacity region, abnormally high atherogenic aerosol concentration may significantly affect cloud physics and precipitation. To investigate the role of aerosol in this extreme event, we conduct a series of simulations using the WRF model coupled with the THOM-Aero scheme. The results offer specific insights on how different levels of aerosol concentration influence cloud microphysics, precipitation formation, and convective intensity for this extreme precipitation case, and the main conclusions are given below.

Firstly, the four simulations with varying initial cloud condensation nuclei (CCN) concentrations reasonably reproduce the spatial pattern of extreme rainfall near Guangzhou, albeit with slight differences in magnitude and maximum rainfall location. In general, higher CCN concentrations tend to decrease the amount of precipitation. Compared to experiment CCNm01 in which the CNN is set to one tenth of the typical maritime values (with a surface CCN at 25 cm^{-3}), the domain total rainfall in experiment CCNc10 whose CNN is set to 10 times of typical continental values (with a surface CCN at 10^4 cm^{-3}) decreases by approximately 10%, and the average hourly rainfall intensity decreases by 1.5–2 mm h^{-1} during the early stage of heavy rainfall. Consistent with the classical aerosol–deep convective cloud interaction theory (Rosenfeld et al., 2008; Fan et al., 2016), more aerosols promote higher cloud droplet number condensation and the release of more latent heating via condensation, thereby stronger updrafts although the enhancement is relatively modest.

Secondly, higher CCN concentration significantly increases cloud droplets number through activation. In experiment CCNc10, the droplet number is two orders of magnitude greater than in CCNm01, while the droplet mass increases by only ~35%, resulting in smaller droplet sizes. This suppresses the auto-conversion process, leading to the fewest raindrops and the least amount of precipitation among all experiments. This suppression of warm-rain formation is consistent with the theoretical framework proposed by Rosenfeld et al. (2008) and Tao et al. (2012). In CCNm01, enhanced auto-conversion combined with limited collection produces smaller raindrops, leading to stronger evaporation and greater rainwater loss, due to the size-dependent evaporation effects (Srivastava and Coen, 1992).

In addition, the less efficient conversion of cloud droplets to rain allows more cloud droplets to be transported to altitudes above the freezing level at the mixed-phase and deep cloud stages, inducing more active ice microphysical processes (including the collection of cloud by snow and graupel, snow deposition and cloud ice transforming into snow) and invigorating convection. These ice microphysical processes increase the mass of snow and graupel, particularly boosting the snow mixing ratio by approximately 25%. However, the impact of aerosols on ice-phase processes is less significant than on warm-rain processes, and has less direct effect on precipitation falling to the ground.

Finally, we point out that the results presented in this paper are based on just one extreme precipitation case. Even though it is a WR case without strong synoptic or mesoscale forcing, the thermal instability in this case is very high and the moisture is also very rich, so that convection is vigorous and accumulated precipitation is extreme (Wu et al., 2020). Such conditions are representative of the environments of many WR cases in south China and therefore should be studied specifically. When forcing is strong but thermodynamic conditions are less favorable, the influence of aerosol concentrations may vary from the conclusions drawn here. Also, the treatment of the aerosol and activation processes in the THOM-Aero scheme is still relatively simple, and the aerosol impacts with more sophisticated schemes and treatments, such as possible coupling of more sophisticated/accurate representation of aerosols and CCN with a spectral BIN microphysics scheme, should be studied when such capabilities and the necessary computational resources are available. Also, due to the lack of direct observations, we only tested several possible aerosol concentration scenarios that span very low maritime concentrations to high continental concentrations. In the future, studies should examine more realistic situations based on observed aerosol concentrations as much as possible.

CRediT authorship contribution statement

Hong Wang: Writing – original draft, Visualization, Methodology, Investigation, Formal analysis, Conceptualization. **Ming Xue:** Writing – review & editing, Supervision, Project administration, Conceptualization. **Jinfang Yin:** Writing – review & editing, Validation, Methodology, Data curation. **Hua Deng:** Validation, Software, Resources.

Declaration of competing interest

The authors declare no conflicts of interest.

Acknowledgement

This study is supported by Guangdong S&T Program (2026B1111020001), Guangdong Meteorological Service Science and Technology Innovation Team (GRMCTD202607-FW03) and the Youth Innovation Team of China Meteorological Administration (CMA2024QN01).

Data availability

The WRF-simulated products, observed rainfall data, and polarimetric radar products used in this study are available on Baidu Netdisk (https://pan.baidu.com/s/1hs_ZjboK_yT-4NAdqP2cTA access code: 73w4). All figures in this manuscript were produced using the *NCAR Command Language (Version 6.6.2) software* (2019).

References

Albrecht, B.A., 1989. Aerosols, cloud microphysics, and fractional cloudiness. Science 245, 1227–1230.
Berry, E.X., Reinhardt, R.L., 1974. An analysis of cloud drop growth by collection Part II: single initial distributions. J. Atmos. Sci. 31, 1825–1831.
Cao, Q., Jiang, B., Shen, X., Lin, W., Chen, J., 2021. Microphysics effects of anthropogenic aerosols on urban heavy precipitation over the Pearl River Delta, China. Atmos. Res. 253, 105478.
Chen, Q., Fan, J., Yin, Y., Han, B., 2020. Aerosol impacts on mesoscale convective systems forming under different vertical wind shear conditions. J. Geophys. Res. Atmos. 125, e2018JD030027.
Chen, T., et al., 2021. Potential impact of aerosols on convective clouds revealed by Himawari-8 observations over different terrain types in eastern China. Atmos. Chem. Phys. 21, 6199–6220.
Dawson, D.T., Xue, M., Milbrandt, J.A., Yau, M.K., 2010. Comparison of evaporation and cold pool development between single-moment and multimoment bulk microphysics schemes in idealized simulations of tornadic thunderstorms. Mon. Weather Rev. 138, 1152–1171.
Fan, J., et al., 2009. Dominant role by vertical wind shear in regulating aerosol effects on deep convective clouds. J. Geophys. Res. Atmos. 114, D22206.
Fan, J., et al., 2012. Aerosol impacts on clouds and precipitation in eastern China: results from bin and bulk microphysics. J. Geophys. Res. Atmos. 117, D00K36.
Fan, J., Wang, Y., Rosenfeld, D., Liu, X., 2016. Review of aerosol–cloud interactions: mechanisms, significance, and challenges. J. Atmos. Sci. 73, 4221–4252.
Feng, L., et al., 2023. Comparison of microphysical characteristics between warm-sector and frontal heavy rainfall in the South of China. J. Trop. Meteorol. 29, 87–100.
Glotfelty, T., Alapaty, K., He, J., Hawbecker, P., Song, X., Zhang, G., 2019. The Weather Research and Forecasting Model with aerosol–cloud interactions (WRF-ACI): development, evaluation, and initial application. Mon. Weather Rev. 147, 1491–1511.
Han, B., Du, Y., Wu, C., Liu, X., 2021. Microphysical characteristics of the coexisting frontal and warm-sector heavy rainfall in South China. J. Geophys. Res. Atmos. 126, e2021JD035446.
Han, X., et al., 2022. Type-dependent impact of aerosols on precipitation associated with deep convective cloud over East Asia. J. Geophys. Res. Atmos. 127, e2021JD036127.
Hong, S.-Y., Noh, Y., Dudhia, J., 2006. A new vertical diffusion package with an explicit treatment of entrainment processes. Mon. Weather Rev. 134, 2318–2341.
Jiang, B., Huang, B., Lin, W., Xu, S., 2016. Investigation of the effects of anthropogenic pollution on typhoon precipitation and microphysical processes using WRF-Chem. J. Atmos. Sci. 73, 1593–1610.
Jiang, J.H., et al., 2018. Contrasting effects on deep convective clouds by different types of aerosols. Nat. Commun. 9, 3874.
Kain, J.S., 2004. The kain–fritsch convective parameterization: an update. J. Appl. Meteorol. 43, 170–181.
Khain, A.P., BenMoshe, N., Pokrovsky, A., 2008. Factors determining the impact of aerosols on surface precipitation from clouds: an attempt at classification. J. Atmos. Sci. 65, 1721–1748.
Lebo, Z., 2018. A numerical investigation of the potential effects of aerosol-induced warming and updraft width and slope on updraft intensity in deep convective clouds. J. Atmos. Sci. 75, 535–554.
Lebo, Z.J., Morrison, H., Seinfeld, J.H., 2012. Are simulated aerosol-induced effects on deep convective clouds strongly dependent on saturation adjustment? Atmos. Chem. Phys. 12, 9941–9964.
Li, Z., Xue, H., Yang, F., 2013. A modeling study of ice formation affected by aerosols. J. Geophys. Res. Atmos. 118, 11,213–11,227.

Li, Z., Rosenfeld, D., Fan, J., 2017. Aerosols and their impact on radiation, clouds, precipitation, and severe weather events. In: Oxford Research Encyclopedia of Environmental Science. Oxford University Press.

Lim, K.-S.S., Hong, S.-Y., 2012. Investigation of aerosol indirect effects on simulated flash-flood heavy rainfall over Korea. Meteorol. Atmos. Phys. 118, 199–214.

Lin, X., Chen, Q., Zou, Z., He, Y., Lu, C., Shu, Z., 2025. The effects of aerosol on the growth of hydrometeors in deep convective clouds. Atmos. Res. 321, 108088.

Liu, Z., Ming, Y., Zhao, C., Lau, N.C., Guo, J., Bollasina, M., Yim, S.H.L., 2020. Contribution of local and remote anthropogenic aerosols to a record-breaking torrential rainfall event in Guangdong Province, China. Atmos. Chem. Phys. 20, 223–241.

Liu, L., Lin, C., Cui, C., Wang, C., Yang, H., Li, S., 2024. Contrasting aerosol effects on shallow and deep convections during the Mei-yu season in China. Atmos. Res. 309, 107599.

Luo, Y., et al., 2017. The Southern China Monsoon Rainfall Experiment (SCMREX). Bull. Am. Meteorol. Soc. 98, 999–1013.

Mlawer, E.J., Taubman, S.J., Brown, P.D., Iacono, M.J., Clough, S.A., 1997. Radiative transfer for inhomogeneous atmospheres: RRTM, a validated correlated-k model for the longwave. J. Geophys. Res. Atmos. 102, 16663–16682.

Morrison, H., Thompson, G., Tatarskii, V., 2009. Impact of cloud microphysics on the development of trailing stratiform precipitation in a simulated squall line: comparison of one- and two-moment schemes. Mon. Weather Rev. 137, 991–1007.

NCAR Command Language (Version 6.6.2) software, 2019. 753 UCAR/NCAR/CISL/TDD, Boulder, Colorado. https://doi.org/10.5065/D6WD3XH5.

Niu, G.-Y., et al., 2011. The community Noah land surface model with multiparameterization options (Noah-MP): 1. Model description and evaluation with local-scale measurements. J. Geophys. Res. 116, D12109.

Ramanathan, V., Crutzen, P.J., Kiehl, J.T., Rosenfeld, D., 2001. Aerosols, climate, and the hydrological cycle. Science 294, 2119–2124.

Rasmussen, K.L., Prein, A.F., Rasmussen, R.M., Ikeda, K., Liu, C., 2020. Changes in the convective population and thermodynamic environments in convection-permitting regional climate simulations over the United States. Climate Dynam. 55, 383–408.

Rosenfeld, D., et al., 2008. Flood or drought: how do aerosols affect precipitation? Science 321, 1309–1313.

Seaman, N.L., Stauffer, D.R., Lario-Gibbs, A.M., 1995. A multiscale four-dimensional data assimilation system applied in the San Joaquin valley during SARMAP. Part I: modeling design and basic performance characteristics. J. Appl. Meteorol. Climatol. 34, 1739–1761.

Srivastava, R.C., Coen, J.L., 1992. New explicit equations for the accurate calculation of the growth and evaporation of hydrometeors by the diffusion of water vapor. J. Atmos. Sci. 49, 1643–1651.

Storer, R.L., van den Heever, S.C., Stephens, G.L., 2010. Modeling aerosol impacts on convective storms in different environments. J. Atmos. Sci. 67, 3904–3915.

Tao, W.-K., Li, X., Khain, A., Matsui, T., Lang, S., Simpson, J., 2007. Role of atmospheric aerosol concentration on deep convective precipitation: cloud-resolving model simulations. J. Geophys. Res. Atmos. 112, D24S18.

Tao, W.-K., Chen, J.-P., Li, Z., Wang, C., Zhang, C., 2012. Impact of aerosols on convective clouds and precipitation. Rev. Geophys. 50, 2011RG000369.

Thompson, G., Eidhammer, T., 2014. A study of aerosol impacts on clouds and precipitation development in a large winter cyclone. J. Atmos. Sci. 71, 3636–3658.

Thompson, G., Field, P.R., Rasmussen, R.M., Hall, W.D., 2008. Explicit forecasts of winter precipitation using an improved bulk microphysics scheme. Part II: implementation of a new snow parameterization. Mon. Weather Rev. 136, 5095–5115.

Twomey, S., 1977. The Influence of pollution on the shortwave albedo of clouds. J. Atmos. Sci. 34, 1149–1152.

Twomey, S.A., Piepgrass, M., Wolfe, T.L., 1984. An assessment of the impact of pollution on global cloud albedo. Tellus B 36B, 356–366.

Wang, H., Kong, F., Wu, N., Lan, H., Yin, J., 2019. An investigation into microphysical structure of a squall line in South China observed with a polarimetric radar and a disdrometer. Atmos. Res. 226, 171–180.

Wang, H., Xue, M., Yin, J., Deng, H., 2023a. Comparison of simulated warm-rain microphysical processes in a record-breaking rainfall event using polarimetric radar observations. J. Geophys. Res. Atmos. 128, e2023JD038742.

Wang, H., Yin, J., Wu, N., Ding, W., 2023b. Microphysical structures of an extreme rainfall event over the coastal metropolitan city of Guangzhou, China: observation analysis with polarimetric radar. Asia-Pac. J. Atmos. Sci. 59, 3–16.

Wu, Z., Cai, J., Lin, L., Hu, S., Zhang, H., Wei, K., 2018. Analysis of mesoscale system and predictability of the torrential rain process in Guangzhou on 7 May 2017. Meteorol. Mon. 44, 485–499 (in Chinese with an English abstract).

Wu, N., Ding, X., Wen, Z., Chen, G., Meng, Z., Lin, L., Min, J., 2020. Contrasting frontal and warm-sector heavy rainfalls over South China during the early-summer rainy season. Atmos. Res. 235, 104693.

Xu, J., Bi, B., Chen, Y., Chen, T., Gong, Y., Li, J., 2018. Mesoscale characteristics and mechanism analysis of the unexpected local torrential rain in Guangzhou on 7 May 2017. Acta. Meteor. Sin. 76, 511–524 (in Chinese with an English abstract).

Yin, J., Zhang, D.-L., Luo, Y., Ma, R., 2020. On the extreme rainfall event of 7 may 2017 over the coastal city of Guangzhou. Part I: impacts of urbanization and orography. Mon. Weather Rev. 148, 955–978.

Zhang, D., Anthes, R.A., 1982. A high-resolution model of the planetary boundary layer—sensitivity tests and comparisons with SESAME-79 data. J. Appl. Meteorol. Climatol. 21, 1594–1609.

Zhang, G., et al., 2010. Impact of anthropogenic emissions and open biomass burning on regional carbonaceous aerosols in South China. Environ. Pollut. 158, 3392–3400.

Zhang, Y., Fan, J., Li, Z., Rosenfeld, D., 2021. Impacts of cloud microphysics parameterizations on simulated aerosol–cloud interactions for deep convective clouds over Houston. Atmos. Chem. Phys. 21, 2363–2381.

Zhao, B., et al., 2018. Impact of aerosols on ice crystal size. Atmos. Chem. Phys. 18, 1065–1078.